# Dielectric Spectroscopy of Single Human Erythrocytes at Physiological Ionic Strength: Dispersion of the Cytoplasm

Jan Gimsa, Torsten Müller, Thomas Schnelle, and Günter Fuhr
Institute of Biology, Humboldt-University, Berlin, Germany

ABSTRACT Usually dielectrophoretic and electrorotation measurements are carried out at low ionic strength to reduce electrolysis and heat production. Such problems are minimized in microelectrode chambers. In a planar ultramicroelectrode chamber fabricated by semiconductor technology, we were able to measure the dielectric properties of human red blood cells in the frequency range from 2 kHz to 200 MHz up to physiological ion concentrations. At low ionic strength, red cells exhibit a typical electrorotation spectrum with an antifield rotation peak at low frequencies and a cofield rotation peak at higher ones. With increasing medium conductivity, both electrorotational peaks shift toward higher frequencies. The cofield peak becomes antifield for conductivities higher than 0.5 S/m. Because the polarizability of the external medium at these ionic strengths becomes similar to that of the cytoplasm, properties can be measured more sensitively. The critical dielectrophoretic frequencies were also determined. From our measurements, in the wide conductivity range from 2 mS/m to 1.5 S/m we propose a single-shell erythrocyte model. This pictures the cell as an oblate spheroid with a long semiaxis of 3.3 $\mu$m and an axial ratio of 1:2. Its membrane exhibits a capacitance of $0.997 \times 10^{-2}$ F/m$^2$ and a specific conductance of 480 S/m$^2$. The cytoplasmic parameters, a conductivity of 0.4 S/m at a dielectric constant of 212, disperse around 15 MHz to become 0.535 S/m and 50, respectively. We attribute this cytoplasmic dispersion to hemoglobin and cytoplasmic ion properties. In electrorotation measurements at about 60 MHz, an unexpectedly low rotation speed was observed. Around 180 MHz, the speed increased dramatically. By analysis of the electric chamber circuit properties, we were able to show that these effects are not due to cell polarization but are instead caused by a dramatic increase in the chamber field strength around 180 MHz. Although the chamber exhibits a resonance around 180 MHz, the harmonic content of the square-topped driving signals generates distortions of electrorotational spectra at far lower frequencies. Possible technological applications of chamber resonances are mentioned.

## INTRODUCTION

In contrast to impedance measurements on suspensions, dielectrophoresis (DP) and electrorotation (ER) do highlight differences in the polarizability of a single particle and its surroundings. These frequency-dependent differences cause the field-induced translational force, $\vec{F}$, and the torque, $\vec{N}$, in DP and ER, respectively. The DP force in a nonuniform electrical field, $\vec{E}$, can be calculated from the field gradient and the real part of the polarization vector, $\vec{P}$:

$$\vec{F} = (\vec{P}\nabla)\vec{E}. \quad (1)$$

When dispersion occurs the polarization vector follows with a delay. In a rotating field ($\vec{E}$), the resulting torque ($\vec{N}$) is proportional to the imaginary part of the polarization vector and is given by the cross-product:

$$\vec{N} = \vec{P} \times \vec{E}. \quad (2)$$

DP and ER allow the determination of dielectric properties of single colloidal particles or cells. Biological applications mainly use the so-called $\beta$-dispersion frequency range to determine specific membrane capacitance, membrane conductance, and cytoplasmic properties (Arnold and Zimmermann, 1982; Pastushenko et al., 1985; Georgiewa et al., 1989; Marszalek et al., 1991; Paul and Otwinowski, 1991; Huang et al., 1992; Kaler et al., 1992; Sokirko, 1992; Gascoyne et al., 1993; Müller et al., 1993; Sukhorukov et al., 1993; Gimsa et al., 1994). Because in ER the torque as well as the counteracting frictional force increase proportionally to the volume, investigations of objects of varying sizes like cells and even macroscopic objects require similar field strengths (Lertes, 1921; Fuhr et al., 1986). Unfortunately, electrode processes, temperature increases, and thermal convection restrict measurements in macroscopic chambers to very low ionic strength.

Recently, microfabricated structures for particle and cell handling as well as for dielectric characterization have been developed (Fuhr et al., 1991; Hagedorn et al., 1992; Huang et al., 1992; Schnelle et al., 1993). The size of the electrodes is now on the order of the particles themselves. The necessary driving voltages decrease with electrode spacing. Furthermore, the surface-volume ratio of the measuring chambers increases, heat dissipation is facilitated, and the problems of temperature increase and convection are drastically reduced. Microchambers allow cell dielectric characterization, even at the ionic strengths used for animal cell culture (Fuhr et al., 1994b,c, 1995).

Until now frequency-independent dielectric parameters for the cytoplasm were assumed when modeling DP and ER. Additional internal dispersions were explained by the

*Received for publication 23 January 1996 and in final form 22 March 1996.*

Address reprint requests to Dr. Jan Gimsa, Institute of Biology, Humboldt-University, Invalidenstrasse 42, D-10115 Berlin, Germany. Tel.: +49-30-28972692; Fax: +49-30-28972520; E-mail: jan=gimsa@rz.hu-berlin.de.



0006-3495/96/07/495/12 $2.00

compartmental structure of the objects, with each compartment characterized by a frequency-independent permittivity and conductivity (Asami et al., 1989; Fuhr et al., 1990; Gimsa et al., 1991; Kakutani et al., 1993). Additional dispersion mechanisms arising from inherent structures were theoretically introduced only for the cytoplasm of thrombocytes (Egger and Donath, 1995). This is astonishing, because the cytoplasm is extremely rich in proteins, and dielectric dispersions of protein suspensions were already extensively discussed in the 1950s (Schwan, 1957; O'Konski, 1960). It is even more astonishing because the superiority of DP and ER over conventional impedance measurements in the particle's parameter resolution is usually stressed. On the other hand, it has been known for a long time that dispersions of proteins are masked by the structural $\beta$-dispersions (Schwan, 1957), the same processes detected by DP and ER. Therefore, dispersions of cytoplasmic proteins were predominantly investigated after cell lysis or in cell free suspensions (Takashima, 1956; Schwan, 1957; Pauly and Schwan, 1966; Takashima and Asami, 1993).

In this paper, a microfabricated four-electrode chamber was used for measurement of the two critical frequencies of the dielectrophoretic spectra where cell movement ceases and the complete electrorotational spectra of human red cells. The whole external conductivity range up to physiological values was examined. Thus it was possible for the first time to exploit the high sensitivity of ER to search for cytoplasmic dispersions at external conductivities at which the polarizabilities of external solution and cytoplasm are comparable. The cytoplasm of human erythrocytes is considered as a model system for these investigations because it has no compartmental structure and can reasonably be considered as a homogeneous hemoglobin suspension.

Dielectric dispersions of protein solutions can be observed as a decrease of the permittivity—the dielectric decrement (Takashima, 1956; Schwan, 1957; Pethig and Kell, 1987). Many efforts were made to relate the observed dispersions to molecular properties (O'Konski, 1960; Takashima, 1993; Takashima and Asami, 1993; Barlow and Thornton, 1986). Dielectric properties of proteins are believed to be important for their physiological function, such as protein-protein association or interaction with charged ligands. Originally, dielectric dispersions were interpreted in terms of field-induced orientation of the protein's permanent dipole moment. To calculate the dipole moment, the distribution of fixed charges on the protein as well as its core bond moment were considered. Later, proton fluctuations were acknowledged as another significant contribution to the observed dipole moment (Orttung, 1968a,b). For hemoglobin in particular, a good theoretical agreement with observed properties was achieved (Takashima, 1993).

Dielectric properties of erythrocytes have been investigated by impedance measurements as well as by DP and ER (Pauly and Schwan, 1966; Takashima et al., 1988; Engel et al., 1988; Asami et al., 1989; Georgiewa et al., 1989; Bao et al., 1992, 1993, 1994; Gimsa et al., 1994; Zhao, 1994; Beving et al., 1994; Becker et al., 1995). Even precise impedance measurements on erythrocytes embedded by mild pressure within a micropore filter did not reveal additional cytoplasmic dispersions in the frequency range up to 10 MHz (Bao et al., 1993). Up to now, DP and ER were not possible at physiological ionic strength for reasons of Joule heating. The use of ultramicroelectrode chambers allows an extension of the conductivity range up to the physiological ionic strength. Because this shifts dielectric dispersions toward high frequencies, we extended the measuring range up to 200 MHz, the highest frequency accessible for our experimental setup. The application of square-topped fields allowed us to separate spectral distortions caused by chamber resonance effects from the frequency dependence of cell polarization.

## MATERIALS AND METHODS

### Erythrocytes

Citrated human blood from healthy donors was supplied by the blood bank (Blutspendedienst im DRK gGmbH, Berlin Buch). It was stored no longer than 5 days in an acid-citrate-dextrose medium at 4°C. For all experiments, the plasma and buffy coat were removed after centrifugation at 500 $\times$ $g$ for 10 min. Then the cells were kept in Krebs-Ringer solution at a hematocrit of about 50%. Under conditions of physiological ionic strength, erythrocytes become crenated (echinocytes) at high pH (Weed and Chailley, 1973; Glaser and Donath, 1984). To reduce crenation, a pH of 6 was used for all experiments. Under these conditions the cells exhibited a biconcave shape. Only in an external conductivity range above 0.5 S/m were they slightly crenated. Within the first 5 min after suspension, an average oblate erythrocyte diameter of 6.6 $\pm$ 0.5 $\mu$m was determined microscopically.

### Sephadex particles

Spherical cross-linked dextran spheres (Sephadex G-15) were purchased from Pharmacia-LKB (Uppsala, Sweden). The dry particles were incubated at room temperature in distilled water (conductivity 0.25 mS/m) for 60 min. After this they were diluted in an electrolyte solution (phosphate-buffered saline) at the conductivity needed for experiments and used within 30 to 120 min.

### Dielectrophoresis and electrorotation measurements

A 300-mOsm solution of sucrose and a 300-mOsm NaCl solution, both containing 1 mM phosphate buffer (pH 6), were appropriately mixed to adjust the conductivity of the measuring solution. For measurements below 12 mS/m, the amount of buffer of the sucrose measuring solution was further reduced. Erythrocytes were suspended to a hematocrit of 0.02%. The conductivity of the suspension was checked after every experiment. Cell translation (DP) or rotation (ER) was investigated in a microchamber by a video microscope system. For DP the two critical frequencies of the spectrum were determined, i.e., the frequencies at which cell movement ceases at zero dielectrophoretic force. These frequencies can be easily measured by adjusting the field frequency to the value at which cell movement toward or away from the electrode edges is balanced (Gimsa et al., 1991). Twenty to thirty-five cells were measured at every medium conductivity. For ER, 6 to 10 complete cell spectra were recorded at every conductivity on sedimented erythrocytes. The cells rotated around their small semiaxis. No frequency-dependent reorientation was observed. The induced rotation speed at the first (antifield) peak was on the order of one revolution per 5 s at a driving voltage of 2 $V_{pp}$. All measurements were

carried out at a room temperature of 23°C within 5 min after suspending the cells in the measuring solution.

## Measuring chamber and external electric field

Erythrocyte and Sephadex experiments were conducted in a four-electrode microchamber (Fig. 1, *A* and *B*). The microelectrode structures were fabricated on quartz glass (Pyrex 7740) by electroplating of gold to a thickness of 950 nm. The chip was mounted on a ceramic chip carrier (Kyocera, Kyoto, Japan) and bonded by 50-$\mu$m gold wires. The carrier could be snapped into a commercial socket. The electrodes were driven by four 90° phase-shifted, symmetrical square-wave signals from a computer-controlled 500-MHz generator (HP 8131A) with 2 $V_{PP}$ amplitude.

## Chamber resonance

Because of the symmetry of the chamber design and the driving signals, the center of the chamber is at a virtual ground potential (see Fig. 1 *C*). The properties of only one electrode can model the electrical chamber behavior (compare to Fig. 7). The series inductance and resistance/capacitance element represent the electrode bond wire and supply strip as well as the electrode surface and measuring volume. In this simple model, resistance and capacitance are determined by the chamber's size and the electrical properties of the aqueous cell suspension. The actual chamber voltage, represented by the voltage across the capacitor/resistor, is frequency independent for low frequencies. For higher frequencies, it increases to a resonance and finally drops to zero (see Fig. 6 *A*). The voltage at resonance decreases with increasing solution conductivities. The electrical chamber properties were analyzed with a Hewlett Packard 4194A impedance analyzer and by measuring the ER of Sephadex particles (see Appendix).

## RESULTS

The first and second critical frequencies (see Fig. 6, *A* and *B*) of DP (about 100 kHz and 100 MHz, respectively) were determined at various external conductivities. At the first critical frequency, negative DP turns positive because of dispersion of membrane polarization (Pastushenko et al., 1985). The second transition is caused by the dispersion of conductivity polarization of cytoplasm and external medium. At the highest frequencies, the DP force is generated from the polarization arising from permittivity differences. Above 0.5 S/m only negative DP was observed. Fig. 2 shows the variation of critical frequencies with external conductivity.

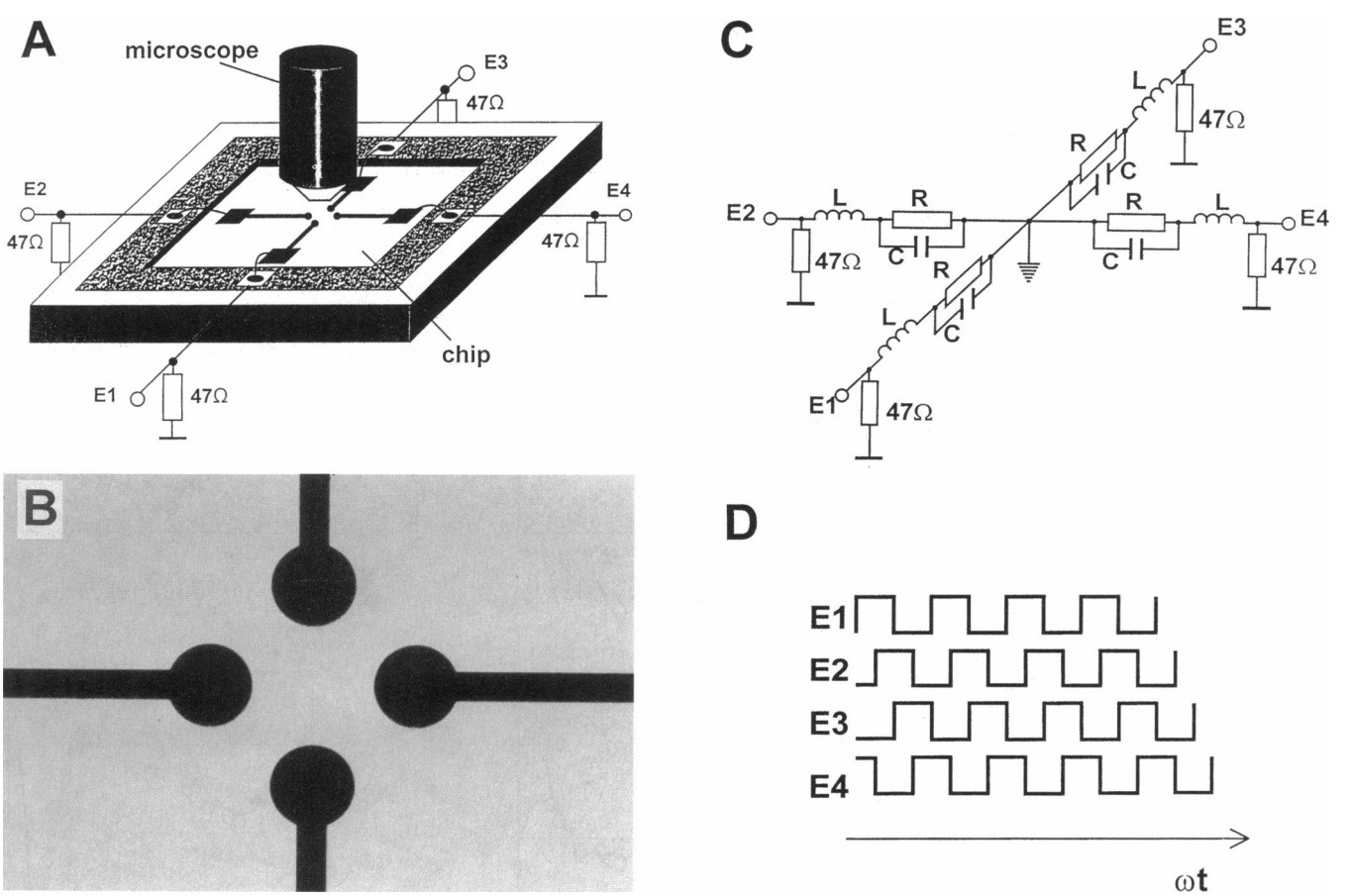


FIGURE 1 (*A*) Micro-structured chamber mounted on a carrier and electrically connected to four generator outputs ($E_1$, $E_2$, $E_3$, $E_4$) for microscopic observation. The four feeding wires were grounded at the socket by 47-Ω resistors. (*B*) Photograph of the measuring volume with the four gold electrodes on a glass wafer. The distance between two opposing electrode tips was 200 $\mu$m. For measurements they were covered about 150 $\mu$m above the electrodes by a glass slip. (*C*) Electronic scheme of the chamber used to model chamber resonances. The center of the scheme is at virtual ground. (*D*) Phase relationship of the driving signals.

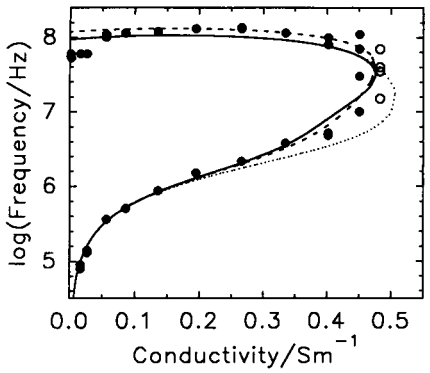


FIGURE 2 The relationship between critical frequency of DP and external conductivity. Unfilled circles represent only 10% of the population at 0.483 S/m. At this conductivity 90% of the cells exhibited positive DP. All curves are based on an oblate cell model with a long half-axis, axis ratio, external permittivity, and membrane capacitance, of 3.3 $\mu$m, 1:2, 78.5, and 0.997 $\times$ $10^{-2}$ F/m$^2$, respectively. The dotted line represents frequency-independent cytoplasmic parameters (a conductivity of 0.535 S/m and a permittivity of 50). In the other two curves a dispersion of the cytoplasmic properties is introduced. The internal permittivity and conductivity were assumed to be 212 and 0.4 S/m ($\sigma_i^0$; see Eq. 4) for low frequencies dispersing around 15 MHz to become 50 ($\epsilon_i^\infty$; see Eq. 3) and 0.64 S/m. The solid curve represents no distribution of the dispersion frequencies ($\alpha = 0$; see Eqs. 2 and 3). For the dashed curve, a distribution of dispersion frequencies around 15 MHz $\alpha = 0.5$ is assumed.

For conductivities below 0.05 S/m, the second critical frequency is ill-defined. In Fig. 2, the lowest frequency value at which cell movement ceased is presented. Above 0.05 S/m definite frequencies could be measured.

In ER the oblate erythrocytes rotated around their axis of symmetry, which aligned perpendicular to the plane of field rotation. Complete ER spectra were measured over the accessible frequency range of 2 kHz to 200 MHz. Fig. 3 presents spectra at four selected conductivities. For higher external conductivities (Fig. 3 *D*), the second peak became antifield. In all cases, for positive or negative rotations the absolute rotation speed drastically increased above 80 MHz, with a peak around 180 MHz. To check whether this behavior reflects actual cell properties or must be attributed to the chamber, Sephadex particles known to possess only a single relaxation were measured (see Appendix). For higher external conductivities when the Sephadex spectra were shifted into the high megahertz range, these particles also exhibited an extraordinarily high rotation peak at 180 MHz. Measured curves differ significantly from the theoretical ones. For erythrocytes and Sephadex particles, only the height depended on the solution conditions; its position did not. All objects exhibited a significant drop of rotation speed at one-third of the peak frequency. Both the peak and the drop could be shifted toward lower frequencies by increasing the inductance of the electrode feed wires (see Appendix). These measurements proved that the observed peak and the drop must be considered distortions of the actual ER spectra.

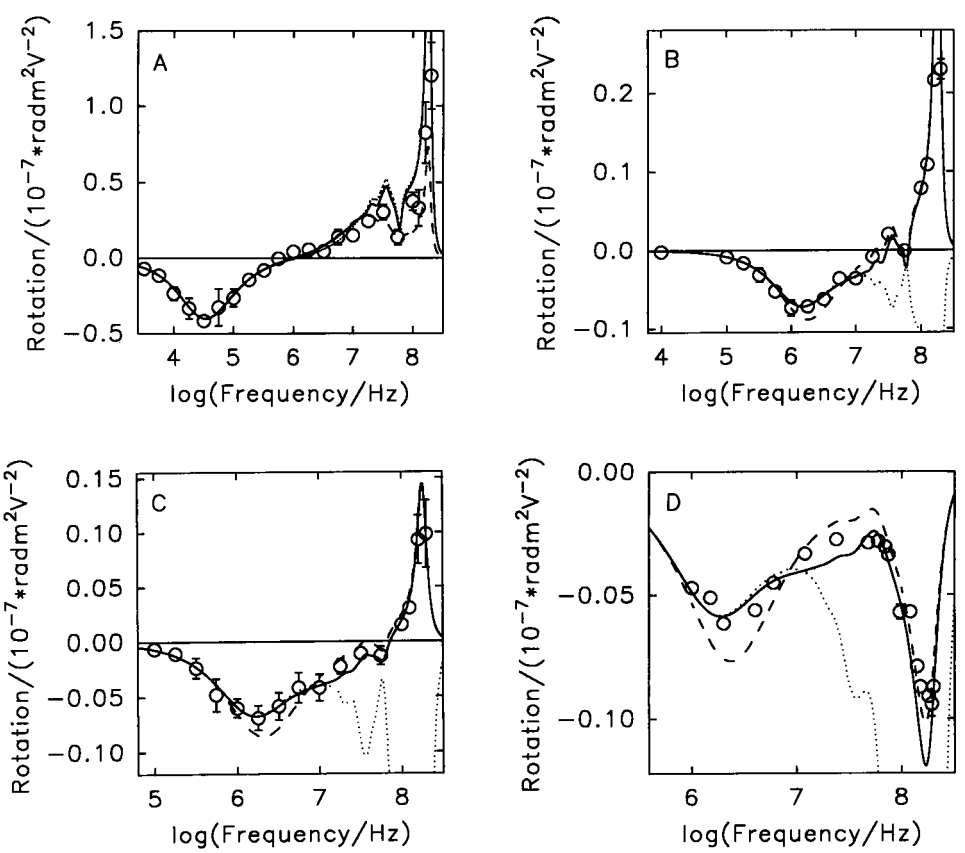


FIGURE 3 Electrorotation spectra of erythrocytes at external conductivities of 1.8 (*A*), 370 (*B*), 640 (*C*), and 1390 (*D*) mS/m. To fit theoretical electrorotation spectra to measured data, the former were normalized to hydrodynamic friction. Cell parameters were assumed as given in Fig. 2. The dotted and dashed curves represent frequency-independent cytoplasmic parameters, a conductivity and a permittivity of 0.4 S/m and 212 (*dashed curves*) as well as 0.535 S/m and 50 (*dotted curves*). The solid curve represents the above properties in combination. The property transition is mediated by the dispersion relation at 15 MHz for $\alpha = 0$.

Peak frequencies and rotation speeds for the first and second ER peaks, at all conductivities measured, are presented in Fig. 4, *A* and *B*, respectively, as well as in Fig. 5, *A* and *B*, respectively. Up to a conductivity of 0.64 S/m the second peak was positive (cofield) and switched to negative above 1 S/m. Between these values rotation was extremely slow (see Fig. 5 *B*). The characteristic frequencies and rotation speeds were obtained by a nonlinear least-squares fit of a Lorentzian curve to the measured points around the peak. To fit the points of the second peak they were first corrected for the chamber resonance. For such corrections, factors for every conductivity and measured frequency above 30 MHz were obtained by comparison of the theoretical rotation spectrum of Sephadex to the measurements (see Appendix). To obtain the theoretical spectra, a spherical model of homogeneous properties (conductivity 0.9 mS/m, permittivity 40) was assumed (Fuhr et al., 1994a). Thus we were able to normalize the second peak and to fit a single Lorentzian curve to the normalized points.

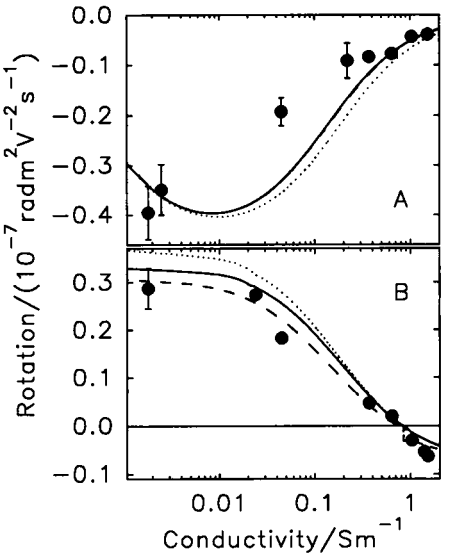


FIGURE 5 Normalized rotation speeds for the first (*A*) and second (*B*) peak (see $R_1$ and $R_2$ in Fig. 6). Dotted, dashed, and solid curves represent the model parameters given in Fig. 2. To correct for friction and field strength, all theoretical peak height curves were normalized by the same factor.

## DISCUSSION

### Influence of measuring conditions on cell properties

When the suspension medium is changed, erythrocytes undergo ionic changes. Cytoplasmic ion concentrations change according to their transmembrane gradients, which in turn changes the transmembrane potential and the osmolarity of the cytoplasm (Glaser and Donath, 1984). Therefore the cell volume may change, even though the measuring solution is isotonic. These processes, which of course depend on the external ionic strength, change the cell's dielectric properties within a few minutes (Glaser and Donath, 1984; Gimsa et al., 1994). To reduce the influence of differing ionic strength at the various external conductivities, all measurements were carried out within 5 min. It is advantageous for dielectric characterization that the membrane area and therefore the overall membrane capacitance remain constant, regardless of volume changes in erythrocytes.

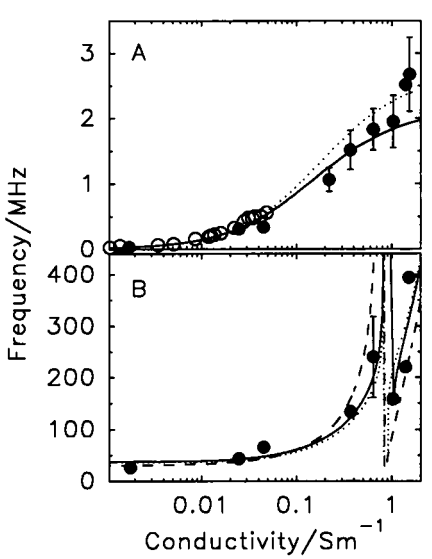


FIGURE 4 Peak frequencies of ER depending on the medium conductivity. Dotted, dashed, and solid curves represent the model parameters given in Fig. 2. (*A*) Frequencies of the first peak ($f_{c1}$; see Fig. 6). Open circles represent data obtained in previous experiments and are taken from Gimsa et al. (1994). Filled circles are new results. (*B*) Frequencies of the second peak ($f_{c2}$). Up to a conductivity of 0.64 S/m rotation was cofield.

### Chamber properties for measurements at high ionic strength

Microtechnology allows the fabrication of chambers with field-inducing electrodes of a size similar to that of biological cells. The cooling efficiency is improved by the increased ratio of surface to heated volume. Although a field strength similar to the one used in macroscopic chambers was applied in the ultramicrochamber, even above 1.5 S/m no excessive thermal convection was observed. Because the amount of gas produced by electrolysis was subcritical for bubble formation, the electrode reaction can be considered reversible for AC currents.

Increasing the ionic strength to physiological values increases the medium conductivity to more than 1.5 S/m and, in turn, strongly shifts the dielectric dispersions toward higher frequencies. Therefore, measurements above 150 MHz become necessary to observe the second rotation peak. At these high frequencies chamber resonances occur. We were able to prove that such distortions of spectra were caused within the microstructure itself (see Appendix). The resonance frequency of the chamber was constant for the

given experimental setup. Only resonance height depended on the external conductivity. A simple electrical model (Fig. 7) allows a qualitative description of the distortions found in the electrorotation spectra for reasonable electrical parameters of the chamber.

Our experiments show that the generation of a constant field strength in DP and ER becomes increasingly complicated for frequencies higher than 100 MHz. One problem is that the cable from the generator must be terminated by a resistor of a matched impedance to ensure a frequency-independent driving voltage. In our case, the terminating resistor was placed at the chip socket. This still leaves the connection through the socket contacts, the bond wires, and the electrode structures on the chip unterminated. The overall length from the resistor to the measuring volume of about 25 mm seems not to be too critical, but one has to keep in mind that the electrodes are surrounded by water with a high permittivity. A proper termination would require resistors integrated into the microstructure. This is barely possible because of Joule heating. These limitations prevent the technical resolution of the problem of increasing the measuring frequency for DP and ER above 200 MHz.

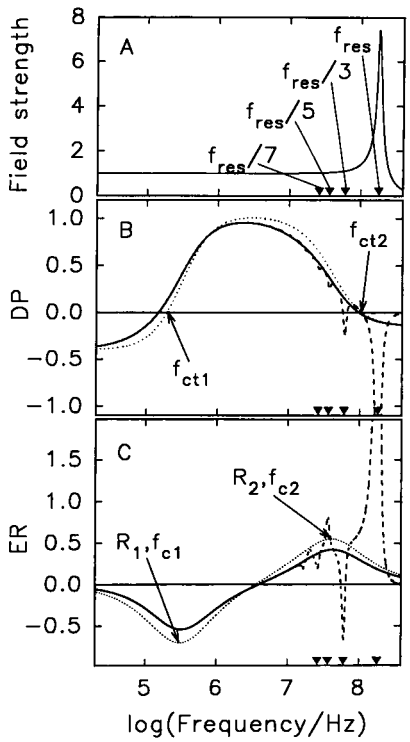


FIGURE 6 (*A*) Plot of the frequency dependence for a harmonic signal of one branch of the model given in Fig. 1. The relative chamber field strength is plotted for a resistance, a capacitance, and an inductance of 7 kΩ, 0.922 pF, and 0.807 μH, respectively. Odd fractions of the resonance frequency are marked. (*B* and *C*) DP and ER spectra, respectively, for sine-wave and square topped fields (key ratio of 1:1) and the influence of a chamber resonance on the spectra in square topped fields (*dotted curves,* sine wave field; *solid curves,* square wave field; *dashed curve,* resonance model, square wave field). All spectra were calculated for the cell parameters of Fig. 2 (dispersion case for $\alpha = 0$) and an external conductivity of 0.05 S/m. As DP and ER, the real and imaginary parts, respectively, of the frequency-dependent term of the induced dipole moment are plotted. The forces for different wave shapes were normalized to $E_{RMS}$.

## The influence of the square-wave signal and the chamber resonance

In Fig. 6 theoretical curves are presented to explain the relations of DP and ER spectra measured in sine and square-wave fields as well as the influence of a chamber resonance. Until now the ER of cells and particles in symmetrical square-wave fields was theoretically described by continuously rotating fields, because it was shown that ER spectra are only slightly perturbed by the higher harmonics. The reason for this is the progressive decrease and the alternating signs of the Fourier components of the torque (see Eq. A2) (Gimsa et al., 1988). Still, it must be stated that in square-wave fields the ER peak frequencies are shifted by about 7% toward higher frequencies (Gimsa et al., 1988). For the first peak this shift results in a calculated membrane capacitance value too low by about the same factor. Continuously rotating sinusoidal fields can no longer be assumed for calculations of the dielectric response of the cells in square-topped fields when resonances occur, as these may amplify higher harmonics (see Appendix). In Figs. 3*A–D*, 8 *B*, and 8 *C* the resonance amplification of the third (around 60 MHz) and fifth harmonics (possessing negative and positive signs, respectively) is obvious.

Without resonances, DP spectra in square-topped fields show stronger deviations from harmonic DP spectra, because every additional Fourier term adds its absolute value to the summated DP force (Gimsa and Glaser, 1992). When critical frequencies are measured in square-wave fields, cell movement stops as the result of balance between all positive and negative dielectrophoretic forces generated by the Fourier terms. Suppose, for example, that the fundamental frequency of the square wave is set at the true second crossover frequency. Then the third and higher harmonics would generate a negative dielectric force. This would cause the experimenter to decrease the frequency and record an erroneously low value. Resonance amplification would not shift the measured critical frequencies in a sine wave field. But in square-topped fields the situation is more complicated. Some of the Fourier terms may be resonance amplified. Therefore the "critical" square wave frequency measured close to the chamber resonance may significantly deviate from the actual value. In Fig. 2 this effect can be seen for the second critical frequency around a conductivity of 0.05 S/m. Lower conductivities yield a much lower second critical frequency than do high ones. This deviation is mainly caused by the negative DP force contribution of the third harmonic. At frequencies above 150 MHz the field strength is amplified by resonance. This causes a significant contribution of the third harmonic to the observed overall DP force for measuring frequencies above 50 MHz. In general, it can be stated that the resonance height and the influence of the third harmonic decreases for increasing external

conductivities. Fig. 6 illustrates theoretically the relations for the measurement of the second critical frequency (frequency-axis intersection) presented in Fig. 2. Square-wave fields shift the zero intersection of the DP force curve slightly toward lower frequencies. Introduction of the resonance changes the function's behavior and may generate additional abscissa intersections of the DP force curve. This behavior can be clearly seen in Fig. 2. Below 0.05 S/m, light damping of the resonance by the solutions of low conductivity resulted in a critical frequency around 60 MHz. Increase of the external conductivity gave increased damping and abolished the additional intersection. This behavior is in accordance with our measurements above 0.05 S/m (Fig. 2).

## The dielectric cell model

The ER spectra measured exhibited two strong relaxation processes (see Fig. 3). These must be attributed to the dispersions of the membrane and cytoplasmic polarization, respectively. We could already show that for human erythrocytes a spheroidal model of rotational symmetry is more suitable than a spherical single-shell model, although it also does not accurately model the cell's shape. Our oblate model had an axial ratio of 1:2, although the biconcave shape of erythrocytes is usually more flat. The reason for this discrepancy is that the curvature at the equatorial zone of the cell is more critical for polarization than the actual axis ratio. In the previous model, internal conductivity, the long half-axis, membrane capacitance, and internal permittivity were fixed at 0.535 S/m, 3.3 $\mu$m, $0.82 \times 10^{-2}$ F/m$^2$, and 50, respectively (Gimsa et al., 1994; for a spheroidal model see Paul and Otwinowski, 1991; Müller et al., 1993). These parameters were obtained from combined measurements of the first critical frequency of DP and the first characteristic frequency of ER in the low external conductivity range up to 40 mS/m. All parameters of the model were in agreement with literature values obtained from independent methods (cytoplasmic conductivity: Pauly and Schwan, 1966; Pilwat and Zimmermann, 1985; cytoplasmic permittivity: Pauly and Schwan, 1966; membrane capacitance: Takashima et al., 1988; Bao et al., 1993). The surface conductivity could be neglected because of the high measuring frequencies (Fuhr and Kuzmin, 1986).

In this paper, the conductivity and frequency ranges for the measurements were widened. Thus it became possible to include the second critical frequency as well as the second ER peak in model considerations. Although resonances were only introduced for ER spectra, the square-wave character of the field was taken into consideration in all calculations. This yielded a correction for the membrane capacitance toward a higher value. A membrane with a permittivity of 9 and an equatorial thickness of 8 nm has a capacitance of $0.997 \times 10^{-2}$ F/m$^2$. This value fits the low-frequency branch of Fig. 2 as well as the first ER peaks at all measured conductivities.

When the ER spectra were corrected for resonances, it became obvious that the low slope of the second peak at 1.8 mS/m (Fig. 3 *A*) as well as the broad continuation of the first, antifield peak toward higher frequencies for medium conductivities (0.37 and 0.64 S/m) (Fig. 3, *B* and *C*) cannot be attributed to the resonance effects. A set of frequency-independent parameters for a single shelled model exhibiting the first and second peaks in the correct positions would require a very high membrane capacitance in combination with a very high internal conductivity. Even this would not allow description of the broadening of the peaks. A similar discrepancy was found for the critical frequencies (Fig. 2). A fit of the high-frequency branch of Fig. 2 requires a very high internal conductivity and the assumption of a very high membrane capacitance for the low frequency branch. Such a parameter set would not reflect the experimental situation, because it would result in a continuation of the two critical frequency branches to conductivities higher than 0.5 S/m (Fig. 2, *dotted curve*). Above 0.45 S/m, only a slight percentage of the population still exhibited positive DP. No critical frequencies were observed above 0.48 S/m. These discrepancies can only be resolved by the introduction of an additional dispersion around 15 MHz. As can be seen from ER (Fig. 3), this dispersion should contribute a negative torque around 10–20 MHz, which cannot be explained within the framework of the common model. To generate this negative torque, polarization currents should disperse to yield displacement currents, a behavior expected from cytoplasmic and membrane proteins or bound cytoplasmic ions. In Figs. 2 and 3 different models are compared. Their parameters were either frequency independent or exhibited a single dispersion or a distribution of dispersions of the cytoplasmic properties around 15 MHz. The dispersing cytoplasmic properties were described by Eqs. 3 and 4:

$$\epsilon_i = \epsilon_i^{\infty} + \Delta\epsilon \frac{1}{1 + (\omega\tau)^{2(1-\alpha)}} \tag{3}$$

$$\sigma_i = \sigma_i^{0} + \Delta\sigma \frac{(\omega\tau)^{2(1-\alpha)}}{1 + (\omega\tau)^{2(1-\alpha)}}. \tag{4}$$

With $\omega$ and $\tau$ presenting the angular frequency of the external field and the time constant of the dispersion process (for parameters see Fig. 2). $\Delta\epsilon$ and $\Delta\sigma$ are related by the well-known dispersion relation. The distribution range of the dispersion frequencies depends on $\alpha$, with a single dispersion frequency being described by $\alpha = 0$ (see Schwan, 1957; Pethig and Kell, 1987). Introduction of a distribution of relaxations drastically improves the fit for the critical frequencies of DP (see Fig. 2, *dashed curve*).

## Electrorotational peak behavior

Results of the dependency of peak frequencies ($f_{c1}$ and $f_{c2}$; see Fig. 6) and peak rotation speeds ($R_1$ and $R_2$) on the external conductivity obtained from the cell spectra are summarized in Figs. 4, *A* and *B*, and 5, *A* and *B*, respectively. Three models are considered in the figures, one with frequency-independent parameters as well as two models

including a dispersion of the cytoplasmic properties at 15 MHz for $\Delta\epsilon = 162$ and $\Delta\sigma = 0.135$ S/m, assuming $\alpha$ to be 0 and 0.5, respectively.

For the $f_{c1}$ behavior (Fig. 4 *A*), no theoretical difference for different $\alpha$ values can be found. In any case, measured peak frequencies above 1 S/m are too high, suggesting a membrane capacitance decreasing around 2 MHz. Because too few measurements are available at the moment, an additional dispersion of the membrane capacitance (possibly caused by membrane proteins) was not introduced into the model. For $f_{c2}$ (Fig. 4 *B*) the introduction of $\alpha$ does not improve the fit. It must be mentioned that the complex frequency behavior around 0.8 S/m cannot be precisely measured because the torque at these conductivities is very small (compare to Fig. 5 *B*).

The rotation speeds obtained over the whole ionic strength range are hardly comparable. Many factors may influence the absolute torque. The viscosity of sucrose solution at 1.8 mS/m drops by about 22% to pure salt solution at 1.5 S/m. In the microchamber, cells could only be measured after sedimentation. Then their surface friction is influenced by glass-membrane interactions depending on time, the ionic strength according to the Derjaguin, Landau, Verwey, Overbeek theory, as well as slight shape changes. Finally it must be assumed that the force transmission from the polarization charges to the cells will also depend on the solution's properties and ionic strength, especially for the first peak.

## Conductive properties of the cytoplasm

To estimate the cytoplasmic DC conductivity of erythrocytes in the physiological state, the cell water can be assumed to occupy 71% of the cell volume (Glaser and Donath, 1984). Ions like $Mg^{2+}$, $HCO_3^-$, as well as hemoglobin add only a small contribution to the conductivity (Pauly and Schwan, 1966). Thus, it is justified to estimate the cytoplasmic DC conductivity from the sum of monovalent ions. The $Na^+$ plus $K^+$ ionic concentration in the whole cytoplasmic volume is about 207 mM. Under the assumption of an ideal electrolyte solution, this concentration yields an internal conductivity of about 1.1 S/m. This is much higher than the cytoplasmic conductivity of about 0.52 S/m that was obtained from the extrapolation of hemolysis experiments at high cell concentrations (Pauly and Schwan, 1966; Georgiewa et al., 1989; Gimsa et al., 1994) or that from impedance measurements (Pauly and Schwan, 1966) or from breakdown experiments (Pilwat and Zimmermann, 1985). These independent methods suggest a hindrance factor of about 2 for DC as well as for AC at about 100 MHz. This factor arises from the hemoglobin concentration. It is known that the hindrance of the mobility of small molecules and ions is very sensitive to hemoglobin concentration and strongly increases with cell shrinkage (Herrmann and Müller, 1986; Gimsa et al., 1994). Therefore, it must be asked whether the extrapolation of the conductivity value to 100% in the lysis experiments reflects the actual cytoplasmatic conductivity or yields an overestimation. Our results suggest a cytoplasmic conductivity of 0.4 S/m at low frequencies; only above 15 MHz does this increase to the value observed in impedance measurements. From these results for DC, it must be concluded that there is a hindrance factor of almost 3. Perhaps, with increasing frequency, displacement currents additionally contribute to the cytoplasmic conductivity, yielding the observed value of 0.535 S/m. It seems reasonable to assume that the ionic mobility is restricted in an elastic fashion, causing such a contribution which, cannot be distiguished from other displacement currents at higher frequencies.

## Contribution of protein dispersions to the cytoplasm properties

The first considerations of the dipole character of molecules led to the conclusion that the dispersion of their orientation will generate a measurable torque in a rotating electric field (Born, 1920; Lertes, 1921). Since then, the dielectric dispersions of small organic dipole molecules (Kirkwood, 1934) as well as of pure protein suspensions have been thoroughly investigated (O'Konski, 1960; Grant et al., 1986; Barlow and Thornton, 1986; Takashima and Asami, 1993). But dispersions have not been introduced into dielectric models of single cells until now. The reason seems to be that the frequency response of cells could be sufficiently well described by assuming frequency-independent model components by expressing response features solely in terms of model structure. Smaller dispersions in the frequency range of 2–20 MHz, in which displacement currents can be caused by proteins, are usually overshadowed by structural dispersions (Schwan, 1957). For the same frequency range, Fuhr et al. (1994b) recently found that the ER torque for protoplasm-rich cells such as fibroblasts or embryo protoplasts in highly conductive solutions is persistently lower than that predicted by reasonable multishelled models. Because the cytoplasm of these cells is highly structured, the authors were not able to attribute this effect to a particular relaxation mechanism. Erythrocytes provide a convenient starting point for theoretical analysis, as their cytoplasm is unstructured and almost exclusively consists of hemoglobin.

Hemoglobin has always been of special interest (Takashima, 1956, 1993; Orttung, 1965, 1968a,b). The cytoplasmic concentration of hemoglobin in erythrocytes is 7 mM (about 450 g/liter) (Pauly and Schwan, 1966; Glaser and Donath, 1984). The dielectric decrement of $\Delta\epsilon = 162$ that we introduced for the cytoplasm is in accordance with the approximation given by Takashima and Asami (1993). But, because of the high cytoplasmatic viscosity it must be assumed that hemoglobin reorientation is highly restricted. This supposedly shifts the dispersion to frequencies below 2 MHz. Therefore, it seems more reasonable to explain the observed dispersion as the orientation of smaller subunits or

side chains. Splitting the molecule into subunits of accordingly smaller dipole moments would increase the frequency of dispersion but still yield a correct dielectric decrement because the latter is proportional to the concentration. Other contributions of similar importance to the decrement of protein suspensions are the ion atmosphere polarization and proton fluctuations (O'Konski, 1960). Furthermore, water bound to protein molecules may contribute to dispersions in the frequency range of 10–20 MHz, because its properties are dramatically changed from that of bulk water (Grant et al., 1986; Pethig and Kell, 1987). These latter contributions are not restricted by the cytoplasmic viscosity as the protein reorientation is. It is clear that our measurements cannot resolve the superposition of these different processes. Therefore, the assumption of a distribution of dispersion frequencies is reasonable.

## CONCLUSION

Cellular changes due to suspension conditions during single-cell, dielectric spectroscopy can be avoided when physiological ionic strength is used. This offers the possibility of measuring sensitive biological systems and medically relevant cells. Such measurements can only be done in microstructured chambers (see also Fuhr et al., 1994c, 1995). Microstructures with unterminated electrodes exhibit resonance phenomena depending on electrode size and arrangement. In our chambers, resonances drastically change the observed electrorotational spectra above 30 MHz and must be considered when calculating dielectric cell and particle data. This can be done either by correction factors obtained from control particles or by electrical chamber models. At first glance, the use of square-wave signals in resonant microstructures seems disadvantageous because ER spectra become even more complicated. However, the observation of ER spectra distortions in square-wave fields at fundamental frequencies far below the chamber resonance allows a separation of chamber and cell properties. In sine wave fields resonances can easily be misinterpreted (see, e.g., Hölzel and Lamprecht, 1987).

For erythrocytes, the ellipsoidal model, first introduced to describe DP and ER in low external conductivity, is also valid at high external conductivities, although our measurements can only be described correctly when cytoplasmic dispersions are introduced. This would not have been necessary if measurements were carried out only at very low or at very high media conductivities. Sweeping the whole conductivity range from below 2 mS/m to above 1.5 S/m revealed the drawbacks of a model with frequency-independent parameters. Measurements in an external conductivity window around the cytoplasmic conductivity are especially sensitive to cytoplasmic dispersions because forces arising from the polarization of the different cell structures are comparably small.

For cell and particle manipulation applications, one can take advantage of chamber resonances. With constant driving voltages at the chamber connectors, resonances may cause a local, extraordinary increase in the chamber field strength and the resulting ponderomotive forces. For such applications suitable models should be developed to predict the electrical behavior of the chambers. This effect seems useful for the construction of ultramicrochambers for cell and particle separation, manipulation, and field caging (Hagedorn et al., 1992; Schnelle et al., 1993; Fuhr et al., 1995). For these applications, increasing the inductance of the feed wires or the addition of capacitive elements will shift the resonance increase of induced forces to lower frequencies.

## APPENDIX: CHARACTERIZATION OF THE ELECTRICAL PROPERTIES OF THE MICROCHAMBER

### Impedance measurements of the chamber properties

To characterize chamber electrode capacitances and resistances, impedance measurements were carried out by a computer-coupled impedance analyzer HP 4194A. In the impedance mode, this device allows measurements up to 40 MHz. For very short connections to the test fixture (HP 16047C) of the impedance analyzer, low-impedance wires were soldered to the wafer contacts of two opposite chamber electrodes. The impedance was measured in the frequency range of 100 kHz to 40 MHz by using different solutions. As in ER experiments, the chamber was covered by a microscopic coverslip. The impedance values were fitted by a nonlinear least-squares procedure to the model presented in Fig. 7. Measurements were made with the chamber filled with air, alcohol, bidistilled water, and a conductivity series of the solutions used for electrorotation experiments. Two dielectrics were assumed to contribute to $C_{ch}$, the filling solution and the chip material itself. Because the thickness of the gold electrode structure was only 950 nm, we assumed $C_{ch}$ to consist of two mirror-inverted structures, one structure with the filling solution as dielectric the other with the chip material (Pyrex 7740 glass). $C_{ch}$ was determined by measurements with air, alcohol, and bidistilled water. Measurements were made in triplicate. The means were used in a linear regression of chamber capacitance versus permittivity of the solutions. The intercept gives the value of the wafer capacitor (0.028 pF, for permittivities of 78.5 for water at 25°C and 5 for Pyrex 7740). The water-filled chamber had a capacitance of 0.461 pF.

For solutions of conductivity greater than 2 mS/m, chamber resistance was inversly proportional to solution conductivity. The constant of proportionality was 1100 $m^{-1}$. This value is below 1400, the value calculated

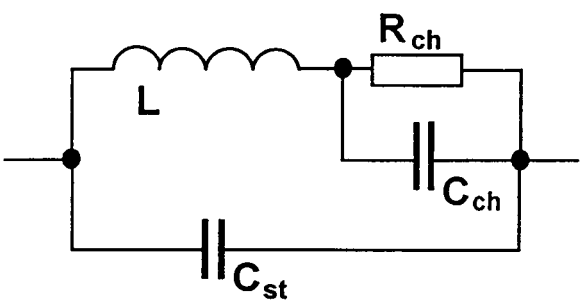


FIGURE 7 Equivalent circuit used to fit the impedance measurements. $C_{st}$ represents the stray capacitance of the test fixture and the connecting wires. $L$, $R_{ch}$, and $C_{ch}$ represent the inductance of the bond wires in series to the electrode strips on the chip, the resistance of the filling solution, and the capacitance formed by the electrodes.

from the permittivity dependence of the capacitance $C_{ch}$. Below 2 mS/m, the observed resistance, $R$, for decreasing conductivities increased much slower than expected. The reason may be surface conductivity effects within the chamber. Because measurements were limited to 40 MHz, only unreproducible values for the inductance, $L$, were obtained.

## Electrorotation measurements with Sephadex control particles

We used an active probe and a 500-MHz HP 54610 oscilloscope to check that the driving voltage at the terminating resistors was frequency independent. Above 40 MHz it was found that higher harmonics slightly distorted the square-topped signal. An increase of the driving voltage around 150 MHz could not be observed. Therefore, the cause of the electrorotational resonance peaks must be located within the chamber structure itself.

Sephadex G15 particles are known to exhibit only single Lorentzian ER peaks (Fuhr et al., 1994a). These peaks are largely independent of the particle radius. The particles can be well described as homogeneous spheres possessing a permittivity and conductivity of 40 and 0.9 mS/m, respectively. In the microchamber, Sephadex spectra were measured at three different external conductivities. Theoretical spectra were calculated using the homogeneous sphere model (Fuhr and Kuzmin, 1986). At the lowest conductivity used, the ER peak was in the frequency range below the observed resonances (Fig. 8 *A*, Table 1). Therefore, it exhibits almost no deviation from the Lorentzian shape. To fit the theoretical spectrum to this measurement only a peak height coefficient for correction of field strength and friction was introduced. At higher conductivities (Fig. 8, *B* and *C*) the measured rotation spectrum clearly does not follow the theoretical predictions. In particular, there is an enormous increase in rotation speed for higher external conductivities at around 180 MHz. For resistors that are not too small, the chamber scheme (Figs. 1 *C* and 7) exhibits a resonance increase of the capacitor voltage with increasing frequency before a final drop (compare to Fig. 6 *A*). The electrorotating particles can be considered as field probes within the capacitor's dielectric liquid. The increase in torque is even more dramatic because it is proportional to the square of the field strength. This idea explains the enormous increase of rotation speed observed at the microchamber's resonant frequency but not the distortions below 100 MHz, e.g., the decrease at 55 MHz (Fig. 8, *B* and *C*).

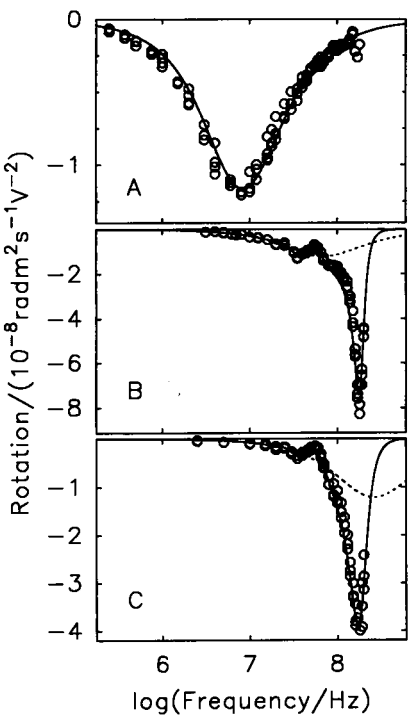


FIGURE 8 Sephadex spectra at three different external conductivities given in Table 1. At each conductivity, measured points were taken from three or four objects. Curve *A* was obtained from the theoretical values using the series development for the torque (Eq. A2) by fitting a factor for the peak height (see Table 1). Dashed lines *B* and *C* are theoretical spectra multiplied by the same peak height coefficient. For the resonance curves inductance and capacitance of the chamber were assumed to be 0.807 μH and 0.922 pF, respectively. The resistance was fitted (see Table 1).

## Influence of square-topped fields on measured spectra

For ER, the generator produces two square-topped fields (in the $x$ and $y$ directions) with duty cycles of 50%. The resulting field can be expressed in a Fourier series:

$$\vec{E} = \frac{4}{\pi} E_0 \Re\left[\begin{pmatrix} 1 \\ j \end{pmatrix}\left(\exp(j\omega t) - \frac{\exp(-j3\omega t)}{3} + \frac{\exp(j5\omega t)}{5} - + \ldots\right)\right]. \quad \text{(A1)}$$

$E$, $E_0$, $j$, $\omega$, and $t$ stand for field vector, maximum field strength, $(-1)^{0.5}$, radian frequency, and time, respectively. This series possesses only odd harmonics and the spinning direction changes for every component. The field strength progressively decreases with every harmonic. The induced dipole moment of the cell can be expressed by the superposition of dipole moments induced by each harmonic (Gimsa et al., 1988). Only the interactions of each harmonic with its own induced dipole are important. Therefore the torque, $\vec{N}$, acting on the particle in a square-topped field, can be developed in a series of torque components that would arise in sinusoidal fields:

$$\vec{N} = \vec{N}(\omega) - \frac{\vec{N}(3\omega)}{9} + \frac{\vec{N}(5\omega)}{25} - + \ldots \quad \text{(A2)}$$

The torque in ER depends on the square of the field strength, so the torques produced by higher harmonics decrease with the square of the Fourier coefficients. In the series, components alternately change their signs and so induce torques with negative and positive spinning directions. Therefore, ER spectra in square-topped fields of a duty cycle of 50% usually show only slight deviations from those in continuously rotating fields (Gimsa et al., 1988). This conclusion is not true when chamber resonances occur. In this case, at some measuring frequencies some harmonics may be at resonance.

Each branch of the scheme in Fig. 1 *C* was assumed to have a capacitance of 0.922 pF, i.e., twice the value obtained from the overall impedance measurements. For a resonance of 180 MHz an inductance of 0.807 μH can be determined. Capacitance and inductance were independent of the solution conductivity. The relatively high inductance can be explained by the fact that the feed wires were partly covered with aqueous solution. Then the only other variable needed to transform the theoretical curves (Fig. 8, *B* and *C, dashed lines*) to fit the resonance points was the resistance, because it determines the height of resonance. Data are given in Table 1. For the resistance a value of about 1 kΩ was found at a conductivity of 1 S/m.

## Influence of increased inductance

As an additional test for the idea of chamber-induced resonances, four SMD (surface-mounted device) coils of 4.7 μH each (purchased from RS Components Ltd., Northants, England) were soldered directly onto the chip carrier. The 4.7 μH SMD has a self-resonance frequency of 35 MHz, which

**TABLE 1 Theoretical peak parameters for homogeneous Sephadex spheres and parameters obtained by spectra fits**

| Figure | Conductivity ($Sm^{-1}$) | Theoretical peak frequency (MHz) | Theoretical peak height as the maximum of the imaginary part of the Clausius-Mossotti factor | Peak height coefficient (rotation divided by theoretical peak height) (rad $m^2 s^{-1} V^{-2}$) | Fitted resistance for one branch of the scheme in Fig. 1 *C* (kΩ) |
|---|---|---|---|---|---|
| A2A | 0.044 | 7.973 | −0.1441 | $8.55 \times 10^{-8}$ | None |
| A2B | 0.370 | 66.352 | −0.1493 | $8.55 \times 10^{-8}$ | 3.09 ± 0.03 |
| A2C | 1.390 | 250.263 | −0.1498 | $8.55 \times 10^{-8}$ | 1.62 ± 0.02 |

suggests that it has a capacity of about 5 pF, enough to swamp the rest of the capacity in the system. Electrically the four coils were switched in series to the electrode connectors. They dramatically shifted the resonance toward lower frequencies. When for ER measurements the same conditions as in Fig. 8 *A* were used, a curve shaped like that of Fig. 8 *B* with a resonance peak frequency of 28.8 MHz was obtained.

The microchambers were a generous gift from Dr. B. Wagner (Fraunhofer Institut für Siliziumtechnologie). We are grateful to Dr. S. Shirley and Mrs. Ch. Mrosek for help with the manuscript.

This work was supported by grant Gi232/1-1 from Deutsche Forschungsgemeinschaft to JG and grants 03120260A and 13 MV03032 from Bundesministerium für Bildung, Wissenschaft, Forschung und Technologie to GF.

## REFERENCES

Arnold, W. M., and U. Zimmermann. 1982. Rotating-field-induced rotation and measurement of the membrane capacitance of single mesophyll cells of *Avena sativa*. *Z. Naturforsch.* 37c:908–915.

Asami, K., Y. Takahashi, and S. Takashima. 1989. Dielectric properties of mouse lymphocytes and erythrocytes. *Biochim. Biophys. Acta.* 1010: 49–55.

Bao, J. Z., C. C. Davis, and R. E. Schmukler. 1992. Frequency domain impedance measurements of erythrocytes. *Biophys. J.* 61:1427–1434.

Bao, J. Z., C. C. Davis, and R. E. Schmukler. 1993. Impedance spectroscopy of human erythrocytes: system calibration and nonlinear modeling. *IEEE Trans. Biomed. Eng.* 40:364–378.

Bao, J. Z., C. C. Davis, and M. L. Swicord. 1994. Microwave dielectric measurements of erythrocyte suspensions. *Biophys. J.* 66:2173–2180.

Barlow, D. J., and J. M. Thornton. 1986. The distribution of charged groups in proteins. *Biopolymers.* 25:1717–1733.

Becker, F. F., X.-B. Wang, Y. Huang, R. Pethig, J. Vykoukal, and P. R. C. Gascoyne. 1995. Separation of human breast cancer cells from blood by differential dielectric affinity. *Proc. Natl. Acad. Sci. USA.* 92:860–864.

Beving, H., L. E. G. Eriksson, C. L. Davey, and D. B. Kell. 1994. Dielectric properties of human blood and erythrocytes at radio frequencies (0.2–10 MHz): dependence on cell volume fraction and medium composition. *Eur. Biophys. J.* 23:207–215.

Born, M. 1920. Über die Beweglichkeit der elektrolytischen Ionen. *Z. Phys.* 1:221–241.

Egger, M., and E. Donath. 1995. Electrorotation measurements of diamide-induced platelet activation changes. *Biophys. J.* 68:364–372.

Engel, J., E. Donath, and J. Gimsa. 1988. Electrorotation of red cells after electroporation. *Stud. Biophys.* 125:53–62.

Fuhr, G., S. Fiedler, T. Müller, Th. Schnelle, H. Glasser, T. Lisec, and B. Wagner. 1994a. Particle micromanipulator consisting of two orthogonal channels with travelling-wave electrode structures. *Sens. Actuat. A.* 41–42:230–239.

Fuhr, G., R. Glaser, and R. Hagedorn. 1986. Rotation of dielectrics in a rotating electric high-frequency field. *Biophys. J.* 49:395–402.

Fuhr, G., H. Glasser, T. Müller, and Th. Schnelle. 1994b. Cell manipulation and cultivation under a.c. electric field influence in highly conductive culture media. *Biochim. Biophys. Acta.* 1201:353–360.

Fuhr, G., R. Hagedorn, T. Müller, W. Benecke, B. Wagner, and J. Gimsa. 1991. Asynchronous traveling-wave induced linear motion of living cells. *Stud. Biophys.* 140:79–102.

Fuhr, G., and P. I. Kuzmin. 1986. Behavior of cells in rotating electric fields with account to surface charges and cell structures. *Biophys. J.* 50:789–795.

Fuhr, G., T. Müller, Th. Schnelle, R. Hagedorn, A. Voigt, S. Fiedler, W. M. Arnold, U. Zimmermann, B. Wagner, and A. Heuberger. 1994c. Radiofrequency microtools for particle and live cell manipulation. *Naturwissenschaften.* 81:528–535.

Fuhr, G., P. Rösch, T. Müller, V. Dressler, and H. Göring. 1990. Dielectric spectroscopy of chloroplasts isolated from higher plants—characterization of the double-membrane system. *Plant. Cell. Physiol.* 31:975–985.

Fuhr, G., Th. Schnelle, R. Hagedorn, and S. G. Shirley. 1995. Dielectrophoretic field cages—a new technique for cell, virus and macromolecule handling. *Cell. Eng.* 1:47–57.

Gascoyne, P. R. C., R. Pethig, J. P. H. Burt, and F. F. Becker. 1993. Membrane changes accompanying the induced differentiation of Friend murine erythroleukaemic cells studied by dielectrophoresis. *Biochim. Biophys. Acta.* 1149:119–126.

Georgiewa, R., E. Donath, and R. Glaser. 1989. On the determination of human erythrocyte intracellular conductivity by means of electrorotation—influence of osmotic pressure. *Stud. Biophys.* 133:185–197.

Gimsa, J., E. Donath, and R. Glaser. 1988. Evaluation of data of simple cells by electrorotation using square-topped fields. *Bioelectrochem. Bioenerg.* 19:389–396.

Gimsa, J., and R. Glaser. 1992. New aspects for theory and and application of dielectrophoresis and electrorotation of biological cells. *In* Biophysics of Membrane Transport. School Proceedings. Part 1. Agricultural University of Wroclaw, Wroclaw, Poland. 156–174.

Gimsa, J., P. Marszalek, U. Löwe, and T. Y. Tsong. 1991. Dielectophoresis and electrorotation of neurospora slime and murine myeloma cells. *Biophys. J.* 60:5–14.

Gimsa, J., Th. Schnelle, G. Zechel, and R. Glaser. 1994. Dielectric spectroscopy of human erythrocytes: investigations under the influence of nystatin. *Biophys. J.* 66:1244–1253.

Glaser, R., and J. Donath. 1984. Stationary ionic states in human red blood cells. *Bioelectrochem. Bioenerg.* 13:71–84.

Grant, E. H., V. E. R. McClean, N. R. V. Nightingale, R. J. Sheppard, and M. J. Chapman. 1986. Dielectric behavior of water in biological solutions: studies on myoglobin, human low-density lipoprotein, and polyvinylpyrrolidone. *Bioelectromagnetics.* 7:151–162.

Hagedorn, R., G. Fuhr, T. Müller, and J. Gimsa. 1992. Travelling-wave dielectrophoresis of microparticles. *Electrophoresis.* 13:49–54.

Herrmann, A., and P. Müller. 1986. Correlation of the internal microviscosity of human erythrocytes to the cell volume and the viscosity of hemoglobin solutions. *Biochim. Biophys. Acta.* 885:80–87.

Hölzel, R., and I. Lamprecht. 1987. Cellular spin resonance of yeast in a frequency range up to 140 MHz. *Z. Naturforsch.* 42c:1367–1369.

Huang, Y., R. Hölzel, R. Pethig, and X.-B. Wang. 1992. Differences in the AC electrodynamics of viable and non-viable yeast cells determined through combined dielectrophoresis and electrorotation studies. *Phys. Med. Biol.* 37:1499–1517.

Kakutani, T., S. Shibatani, and M. Senda. 1993. Electrorotation of barley mesophyll protoplasts. *Bioelectrochem. Bioenerg.* 31:85–97.

Kaler, K. V. I. S., J.-P. Xie, T. B. Jones, and R. Paul. 1992. Dual-frequency dielectrophoretic levitation of canola protoplasts. *Biophys. J.* 63:58–69.

Kirkwood, J. G. 1934. Theory of solutions of molecules containing widely separated charges with special application to zwitterions. *J. Chem. Phys.* 2:351–361.

Lertes, P. 1921. Der Dipolrotationseffekt bei dielektrischen Flüssigkeiten. *Z. Phys.* 6:56–68.

Marszalek, P., J. J. Zielinsky, M. Fikus, and T. Y. Tsong. 1991. Determination of electric parameters of cell membranes by a dielectrophoresis method. *Biophys. J.* 59:982–987.

Müller, T., L. Küchler, G. Fuhr, T. Schnelle, and A. Sokirko. 1993. Dielektrische Einzelzellspektroskopie an Pollen verschiedener Waldbaumarten—Charakterisierung der Pollenvitalität. *Silvia Genet.* 42: 311–322.

O'Konski, C. T. 1960. Electric properties of macromolecules. V. Theory of ionic polarization in polyelectrolytes. *J. Phys. Chem.* 64:605–619.

Orttung, W. H. 1965. Evidence for a permanent dipole moment in hemoglobin from Kerr effect optical dispersion. *J. Am. Chem. Soc.* 87: 924–926.

Orttung, W. H. 1968a. Anisotropy of proton fluctuations and the Kerr effect of protein solutions. Theoretical considerations. *J. Chem. Phys.* 72:4058–4066.

Orttung, W. H. 1968b. Anisotropy of proton fluctuations in proteins. Calculations for simple models. *J. Chem. Phys.* 72:4066–4071.

Pastushenko, V. Ph., P. I. Kuzmin, and Yu. A. Chizmadshev. 1985. Dielectrophoresis and electrorotation: a unified theory of spherically symmetrical cells. *Stud. Biophys.* 110:51–57.

Paul, R., and M. Otwinowski. 1991. The theory of the frequency response of ellipsoidal biological cells in rotating electrical fields. *J. Theor. Biol.* 148:495–519.

Pauly, H., and H. P. Schwan. 1966. Dielectric properties and ion mobility in erythrocytes. *Biophys. J.* 6:621–639.

Pethig, R., and D. B. Kell. 1987. The passive electrical properties of biological systems: their significance in physiology, biophysics and biotechnology. *Phys. Med. Biol.* 32:933–977.

Pilwat, G., and U. Zimmermann. 1985. Determination of intracellular conductivity from electrical breakdown measurements. *Biochim. Biophys. Acta.* 820:305–314.

Schnelle, Th., R. Hagedorn, G. Fuhr, S. Fiedler, and T. Müller. 1993. Three-dimensional electric field traps for manipulation of cells—calculation and experimental verification. *Biochim. Biophys. Acta.* 1157: 127–140.

Schwan, H. P. 1957. Electrical properties of tissue and cell suspensions. *Adv. Med. Biol. Phys.* 5:147–209.

Sokirko, A. V. 1992. The electrorotation of axisymmetrical cell. *Biol. Mem.* 6:587–600.

Sukhorukov, V. L., W. M. Arnold, and U. Zimmermann. 1993. Hypotonically induced changes in the plasma membrane of cultured mammalian cells. *J. Membr. Biol.* 132:27–40.

Takashima, S. 1956. Dielectric properties of hemoglobin. I. Studies at 1 megacycle. *J. Am. Chem. Soc.* 78:541–546.

Takashima, S. 1993. Use of protein database for the computation of the dipole moments of normal and abnormal hemoglobins. *Biophys. J.* 54:995–1000.

Takashima, S., and K. Asami. 1993. Calculation and measurement of the dipole moment of small proteins: use of protein data base. *Biopolymers.* 33:59–68.

Takashima, S., K. Asami, and Y. Takahashi. 1988. Frequency domain studies of impedance characteristics of biological cells using micropipette technique. *Biophys. J.* 54:995–1000.

Weed, R. I., and B. Chailley. 1973. Calcium-pH interactions in the production of shape change in erythrocytes. *In* Red Cell Shape. M. Bessis, R. I. Weed, and P. F. Leblond, editors. Springer Verlag, New York. 55–68.

Zhao, T.-X. 1994. Contributions of suspending medium to electrical impedance of blood. *Biochim. Biophys. Acta.* 1201:179–185.